

X-ray Photoelectron Spectroscopy in the Analysis of Titanium and Palladium Nanolayers

G. WESOŁOWSKI^{a,*}, A. KUBALA-KUKUŚ^a, D. BANAŚ^a, K. SZARY^a,
I. STABRAWA^a, A. FOKS^a, Ł. JABŁOŃSKI^a, P. JAGODZIŃSKI^a, M. PAJEK^a,
R. STACHURA^a, D. SOBOTA^a, M. BORYSIEWICZ^b AND O. SADOWSKI^b

^a*Institute of Physics, Jan Kochanowski University, Uniwersytecka 7, 25-406 Kielce, Poland*

^b*Lukasiewicz Research Network — Institute of Microelectronics and Photonics, al. Lotników 32/46, PL-02668 Warszawa, Poland*

Doi: [10.12693/APhysPolA.145.101](https://doi.org/10.12693/APhysPolA.145.101)

*e-mail: s131403@student.ujk.edu.pl

In the presented study, X-ray photoelectron spectroscopy and total reflection X-ray photoelectron spectroscopy methods were applied to analyze the Ti (75 nm) and Pd (100 nm) nanolayers deposited on the Si substrate using magnetron sputtering. The aim of the research was to determine the elemental composition and surface homogeneity of the analyzed nanolayers before their irradiation with highly charged xenon ions and to estimate the detection limit of the X-ray photoelectron spectroscopy technique for various glancing angles. The measurements were conducted using the SPECS mono-XPS system in the Institute of Physics at the Jan Kochanowski University (Kielce, Poland). The experimental setup and measurement conditions for the studied Ti and Pd layers are described. The X-ray photoelectron spectroscopy spectra were registered both for the non-total (35° and 10° angles) and total reflection (2.2° for the Pd nanolayer and 1.5° for the Ti nanolayer) regimes. The position of the C 1s photoelectron peak was applied (C-C component, binding energy 284.8 eV) to calibrate energy. First, the homogeneity of the nanolayers was investigated. The analysis of spectra concentrated on investigating the photoelectron peaks and, consequently, on determining the following: the binding energy of electrons, the intensity and full width at half maximum of photoelectron peaks, the background level, and the elemental composition of the nanolayer surface. In this study, the detection limit of the X-ray photoelectron spectroscopy measurements for different photoelectron peaks was calculated in relation to the excitation angle. An improvement of the X-ray photoelectron spectroscopy detection limit by a factor of 3–6, depending on the type of photoelectron peak, was observed for the angles below the critical angle of the X-ray total reflection phenomenon.

topics: Ti and Pd nanolayers, X-ray photoelectron spectroscopy (XPS), total reflection XPS

1. Introduction

X-ray photoelectron spectroscopy (XPS) is a surface analysis technique in which a low-energy X-ray beam is directed toward the studied sample, which leads to emitting electrons from the surface. Analyzing the registered energy spectra of the electrons provides information about such properties of the surface as qualitative and quantitative elemental composition, surface homogeneity, and the chemical environment of elements [1, 2]. The sensitivity of the X-ray photoelectron spectroscopy technique can be improved by applying the phenomenon of total reflection of X-ray radiation when the excitation beam is directed at the analyzed sample at an angle smaller than the critical angle [3]. This type of the modified technique is known as the total reflection X-ray photoelectron spectroscopy (TRXPS) [4–8]. Under the total reflection geometrical condition, primary X-rays cannot penetrate

deeply into the analyzed sample. The intensity of X-rays in the evanescent range can be as much as four times stronger compared to the intensity of the primary X-ray beam. This is caused by forming a standing wave on the surface [4]. Consequently, the photoelectron signal is increased with simultaneous background reduction, which is also caused by a lower inelastic scattering of electrons [4]. Specific aspects of measurement geometry in the regime of total external reflection of X-ray is physical basis of low-angle X-ray spectroscopy, diffraction, and reflectometry techniques such as total reflection X-ray fluorescence (TXRF) [3], grazing incidence X-ray fluorescence (GIXRF) [3], grazing emission X-ray fluorescence (GEXRF) [3, 9, 10], grazing incidence X-Ray diffraction (GIXRD) [11], and the X-ray reflectometry [12]. These techniques are often used to analyze nanolayers, which facilitates determining various properties of sample surfaces, e.g., elemental and chemical composition, morphology, density,

thickness, roughness, and depth profile, also by our atomic physics and nanophysics group, in different applications [3, 13–15].

The research conducted by our group focuses on studying the processes of forming surface nanostructures in the interaction of highly charged xenon ions with nanolayers using the Kielce EBIS facility of the Jan Kochanowski University (Kielce, Poland) [16]. Research centers on metallic (Au, Ti) nanolayers [15, 17] as well as the dependence of nanostructure sizes on the kinetic and potential energy of the Xe ions. In order to continue the study for other metallic nanolayers (with different thickness values) and to interpret the results correctly, it is necessary to know the properties of the nanolayers obtained by applying X-ray photoelectron spectroscopy with the best possible detection limit.

In the presented studies, the XPS technique was applied to analyze titanium (Ti) and palladium (Pd) nanolayers deposited on the silicon (Si) substrate. In the case of titanium, the nanolayer thickness was 75 nm, whereas for palladium, it was 100 nm. The analysis was conducted both in the non-total and total X-ray reflection conditions. In the presented studies, titanium and palladium were selected for the research of nanolayer surface modifications in interaction with highly charged Xe ions, but in general, Ti and Pd materials are commonly used in various applications [18–21].

The paper begins with a description of the experimental setup, the measurement conditions, and the analyzed samples. Calculating the critical angle of the total X-ray reflection is also discussed. Next, the results and discussion section is presented. At the beginning of the section, the XPS survey spectra are presented for different regions of the nanolayer surface. Analyzing the spectra concentrates on interpreting photoelectron and Auger peaks as well as on determining the nanolayer surface elemental composition. Furthermore, surface homogeneity is discussed. Comparing the spectra registered for different glancing angles (both for the Ti and Pd nanolayers) is an important aspect of the study. In this case, analyzing the spectra focuses on determining the binding energy of electrons, the intensity and the full width at half maximum (FWHM) of photoelectron peaks, the background level, and the elemental composition of the nanolayer surface. This, in turn, enables the specification of the XPS/TRXPS detection limit for various photoelectron peaks.

2. Experiment

2.1. Samples description

The research included analyzing titanium (Ti) and palladium (Pd) layers (75 nm and 100 nm in thickness, respectively). The layers were deposited on a silicon (Si) wafers, standard $\langle 111 \rangle$ orientation) substrate. The samples were prepared at the

Lukasiewicz Research Network Institute of Microelectronics and Photonics in Warsaw, Poland, using magnetron sputtering in the thin film deposition system (TFDS) from VST Ltd. The preparation process was performed in the conditions of high vacuum ($4\text{--}5 \times 10^{-7}$ Pa). 4N purity materials were used as the targets. In this process, the deposition rate was 2 nm per second. The size of the prepared samples was 10 mm, 5 mm, and 1 mm in length, width, and thickness, respectively. The layer thickness was verified using a surface profilometer, DekTak 150 (Veeco Instruments Inc.).

2.2. Experimental setup and measurement conditions

The X-ray photoelectron spectroscopy and the total reflection X-ray photoelectron spectroscopy measurements were performed with the SPECS mono-XPS system using monochromatized Al K_α radiation with an energy of 1486.7 eV emitted from an XR-50 M high-intensity twin anode (Al, Ag) X-ray source optimized for XPS experiments. The X-ray tube (300 W) was operated with a voltage $U = 15$ kV and current $I = 20$ mA. The X-ray beam monochromatization was performed with a quartz single-crystal mirror monochromator with a 500 mm Rowland circle and a rocking curve width of approximately 160 meV.

The XPS and TRXPS spectra were obtained utilizing a PHOIBOS 100 electron energy analyzer equipped with a one-dimensional delayline detector (1D-DLD). The vacuum chamber pressure was about 10^{-9} mbar. The pass energy of 30 eV was selected to analyze the nanolayers under both non-total and total X-ray reflection conditions. Spectrometer calibration was checked using the Ag reference foil (Goodfellow), applied for analyzing two photoelectron peaks: Ag $3d_{3/2}$ and Ag $3d_{5/2}$. The position of the Ag $3d_{3/2}$ peak was 374.3 eV, whilst for Ag $3d_{5/2}$, it was 368.4 eV, matching the reference values [22]. The FWHM of Ag $3d$ peaks was 1 eV. The Pd and Ti nanolayer samples studied with the TRXPS measurements were automatically tilted with a manipulator, standard LN2 1.5, a device offering three-axes (x, y, z) and two-angular (polar, azimuth) movements. The polar rotation precision equaled 0.05° . The measurements also involved charge compensation, achieved with the assistance of a flood gun FG-500. The following values were applied for the Pd nanolayer: electron energy of 0.4 eV, emission current of $4 \mu\text{A}$. In the case of the Ti nanolayer, these values were 0.7 eV for electron energy and $15 \mu\text{A}$ for the emission current.

2.3. Critical angle of total X-ray reflection

TRXPS measurements require selecting the measurement angle (i.e., the glancing angle), which has to be below the critical angle, which is characteristic

for a given X-ray beam energy and the type of the reflecting surface (nanolayers). The critical angle can be calculated from the following equation

$$\theta_c = C \sqrt{\frac{Z \rho}{A}} \frac{1}{E}, \quad (1)$$

where Z , A , and ρ [g/cm³] are the atomic number, the mass number, and the surface material density, respectively; E [keV] is the X-ray energy, and C is a constant equal to 1.65 for the assumed units of the discussed physical quantities. Taking into account the energy of Al K_{α} X-ray (1486.7 eV), used as the excitation radiation in XPS/TRXPS measurements, the critical angle for Ti is 1.60° and for Pd is 2.37° [23]. A relatively high value of the critical angles, compared to the values applied in the low-angle spectroscopy, is a consequence of the low energy of the X-ray beam. In the presented studies, the XPS measurements were performed for the following angles: 35° and 10° (Pd and Ti nanolayers), 2.2° (Pd nanolayers, X-ray total reflection condition) and 1.5° (Ti nanolayers, X-ray total reflection condition).

3. Result and discussion

3.1. Survey spectra. Surface homogeneity

The homogeneity of the nanolayer surface was established by measuring the XPS survey spectra at an angle of 35° for five areas on the sample (i.e., the center and four corners of the sample). Figure 1

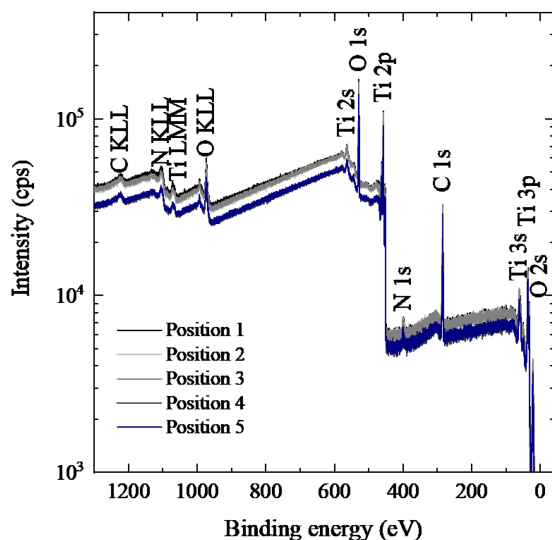


Fig. 1. XPS survey spectra of Ti 75 nm nanolayer deposited on the silicon (Si) substrate for five areas on the sample measured at a glancing angle of 35°. The sample was irradiated by the monochromatized Al K_{α} photons. In the spectra, both photoelectron (Ti 2s, O 1s, Ti 2p, N 1s, C 1s, Ti 3s, Ti 3p, O 2s) and Auger peaks (C-KLL, N-KLL, Ti-LMM, O-KLL) were identified.

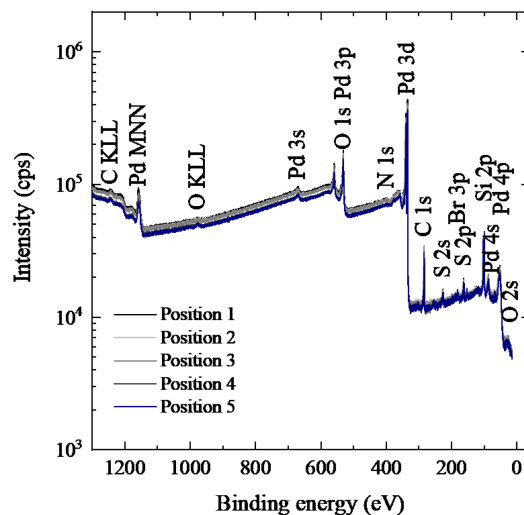


Fig. 2. XPS survey spectra of Pd 100 nm nanolayer deposited on the silicon (Si) substrate for five areas on the sample measured at a glancing angle of 35°. The sample was irradiated by the monochromatized Al K_{α} photons. In the spectra, both photoelectron (Pd 3s, Pd 3p, O 1s, N 1s, Pd 3d, C 1s, S 2s, Br 3p, S 2p, Si 2p, Pd 4s, Pd 4p, O 2s) and Auger peaks (C-KLL, Pd-MNN, O-KLL) were identified.

presents the XPS survey spectra registered for the Ti nanolayer (75 nm) deposited on the silicon. The survey spectra were measured in the electron binding energy range from 0 to 1300 eV. The energy step was 0.1 eV, and the dwell time was 0.1 s. For energy calibration, the position of the C 1s photoelectron peak was applied (C-C component, binding energy 284.8 eV). In the spectra, both photoelectron (O 1s, Ti 2s, Ti 2p, N 1s, C 1s, Ti 3s, Ti 3p, O 2s) and Auger peaks (C-KLL, N-KLL, Ti-LMM, O-KLL) were identified. In the spectrum, the photoelectron Ti 2p peak was registered as Ti 2p_{1/2} and Ti 2p_{3/2} splitting. A detectable quantity of adventitious carbon contamination was observed in the sample due to its exposition to the atmosphere. Similarly, the presence of adventitious nitrogen from air exposure could be observed in the spectra, however, the observed amount was considerably smaller.

In the case of oxygen, this element is present on the samples due to the exposition to the atmosphere, either due to adventitious contamination, oxidation, or water.

Figure 2 presents the XPS survey spectra of the Pd nanolayer (100 nm) deposited on the silicon measured at the angle of 35° for five areas on the sample. The survey spectra were measured in the electron binding energy range from 0 to 1300 eV. The measured energy step was 0.1 eV, and the dwell time was 0.1 s. In the spectra, both the photoelectron (Pd 3s, Pd 3p, O 1s, N 1s, Pd 3d, C 1s, S 2s, Br 3p, S 2p, Si 2p, Pd 4s, Pd 4p, O 2s) and Auger peaks (C-KLL, Pd-MNN, O-KLL) were identified. Moreover, the following splitting was

TABLE I

Element concentrations [at.%] on Pd and Ti surface nanolayers for five various regions of the nanolayer surface measured at an angle of 35° . The table presents element concentration mean values, standard deviations, and the coefficients of variation.

Elements	Concentration [at.%]					Mean value [at.%]	Standard deviation [at.%]	Variation coefficient [%]
	Position 1	Position 2	Position 3	Position 4	Position 5			
100 nm palladium nanolayer								
Palladium	41.2	41.6	41.6	29.6	31.3	37.1	5.4	14.7
Silicon	23.3	22.2	15.5	36.6	36.7	26.8	8.4	31.3
Carbon	18.4	20.8	24.3	18.3	17.4	19.8	2.5	12.7
Oxygen	9.7	8.4	10.8	8.9	8.6	9.3	0.9	9.5
Sulfur	4.0	3.4	3.8	3.1	3.2	3.5	0.3	9.7
Nitrogen	3.1	2.9	3.4	2.9	2.2	2.9	0.4	13.4
Bromine	0.4	0.8	0.6	0.7	0.7	0.6	0.1	20.7
75 nm titanium nanolayer								
Oxygen	46.9	45.7	45.3	45.5	45.5	45.8	0.6	1.3
Carbon	25.8	28.5	28.5	28.7	28.3	28.0	1.1	3.9
Titanium	25.7	24.7	24.9	23.9	24.8	24.8	0.6	2.3
Nitrogen	1.6	1.2	1.3	1.9	1.4	1.5	0.2	16.8

noticed: Pd $3p_{1/2}$ and Pd $3p_{3/2}$, Pd $3d_{3/2}$ and Pd $3p_{5/2}$, Pd $4p_{1/2}$ and Pd $4p_{3/2}$. Additionally, the overlapping of the Pd $3p_{3/2}$ and the O $1s$ photoelectron peaks was observed as well.

Similarly to the survey spectrum of titanium, elements originating from the atmosphere are visible (C, N, O). Furthermore, elements such as bromine (Br), sulfur (S), and silicon (Si) can be observed as well. The presence of the silicon photoelectron peak (from the silicon substrate) in the recorded XPS spectra is evidence that the Pd layer is not uniform.

The registered survey spectra were used to identify the elemental composition of the studied nanolayers. The quantitative analysis of elemental composition was performed with the CasaXPS software. Table I presents element concentrations [at.%] on the Pd and Ti surface nanolayers for various positions and the calculated mean values, standard deviations, and coefficients of variation [%]. For the Pd nanolayer surface, the following mean element concentrations were obtained: palladium (37.1 at.%), silicon (26.8 at.%), carbon (19.8 at.%), oxygen (9.3 at.%), sulfur (3.5 at.%), nitrogen (2.9 at.%), and bromine (0.6 at.%). Standard deviations were in the range from 0.1 at.% (Br) to 8.4 at.% (Si), resulting in a variation coefficient at the level of 10–30%. The most significant concentration variation was noticed for silicon (31%), while the Pd concentration changed by about 15%.

For the Ti nanolayer surface, the following mean composition was obtained: oxygen (45.8 at.%), carbon (28.0 at.%), titanium (24.8 at.%), and nitrogen (1.5 at.%). Standard deviations were in the range from 0.2 at.% (N) to 1.1 at.% (C), resulting in a variation coefficient at a level of 1–17%. The largest variation in concentration was observed for nitrogen (16.8%), while the Ti concentration changed within 2%.

Comparing the results for the Ti and Pd nanolayers, it can be seen that the coefficient of variation is particularly greater when evaluating elemental concentrations within the sample of palladium nanolayers. This suggests that the Pd nanolayer sample shows a certain degree of surface heterogeneity, which is probably influenced by the sputtering parameters.

3.2. Comparison of spectra for different glancing angles

In the presented study, the X-ray photoelectron spectroscopy was applied both in non-total and total reflection of primary X-ray beam conditions in order to compare between XPS and TRXPS techniques signal-to-noise ratio determining the detection limit. Applying the TRXPS method should improve the value of the element detection limit.

In order to investigate the relationship between the detection limit and the incidence angle, spectra for three angles were collected, namely the typical XPS glancing angle (35°) and the intermediate value of angle (10°) for both samples, and an angle value below the critical angle (2.2° for Pd and 1.5° for Ti), for the center area on the samples.

Figures 3 and 4 present the XPS and TRXPS survey spectra of the Ti nanolayer (75 nm) and Pd nanolayer (100 nm), respectively, deposited on the silicon (Si), for different glancing angles. The decrease in the intensities of the TRXPS spectra compared to those at intermediate angles is related to the change in the primary beam area on the sample surface for different angles.

Table II presents element concentrations [at.%] on the Pd and Ti surface nanolayers obtained from survey spectra registered for the following angle values: 35° , 10° , 2.2° (Pd), and 1.5° (Ti). In addition, Table II also provides element concentration mean

TABLE II

Element concentrations [at.%] on the Pd and Ti surface nanolayers obtained from survey spectra registered for angle values of 35°, 10°, 2.2°(Pd), and 1.5°(Ti). The table shows element concentration mean values, standard deviations, and the coefficients of variation.

Elements	Concentration [at.%]				Mean value [at.%]	Standard deviation [at.%]	Variation coefficient [%]
	angle 35°	angle 10°	angle 2.2°	angle 1.5°			
100 nm palladium nanolayer							
Palladium	40.1	37.5	35.6	–	37.7	2.3	6.0
Silicon	20.5	22.7	24.7	–	22.6	2.1	9.2
Carbon	25.3	26.4	27.4	–	26.4	1.1	4.1
Oxygen	6.2	5.3	4.9	–	5.5	0.7	12.1
Sulfur	4.2	4.2	3.9	–	4.1	0.2	4.7
Nitrogen	3.5	3.7	3.3	–	3.5	0.2	5.7
Bromine	0.28	0.20	0.26	–	0.25	0.04	16.9
75 nm titanium nanolayer							
Oxygen	45.4	45.3	–	43.7	44.8	0.95	2.1
Carbon	26.5	29.1	–	32.4	29.3	3.0	10.2
Titanium	27.1	24.5	–	22.4	24.7	2.4	9.3
Nitrogen	1.1	1.2	–	1.4	1.2	0.15	12.5

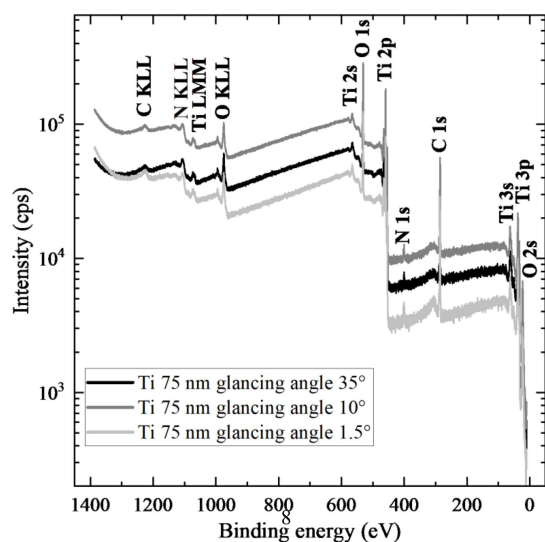


Fig. 3. XPS survey spectra of Ti 75 nm nanolayer deposited on the silicon (Si) substrate for different glancing angles: 35°, 10°, and 1.5° (below the critical angle for Ti (1.60°)). The sample was irradiated by the monochromatized Al K_{α} photons. In the spectra, both photoelectron (O 1s, Ti 2s, Ti 2p, N 1s, C 1s, Ti 3s, Ti 3p, O 2s) and Auger peaks (C-KLL, N-KLL, Ti-LMM, O-KLL) were identified.

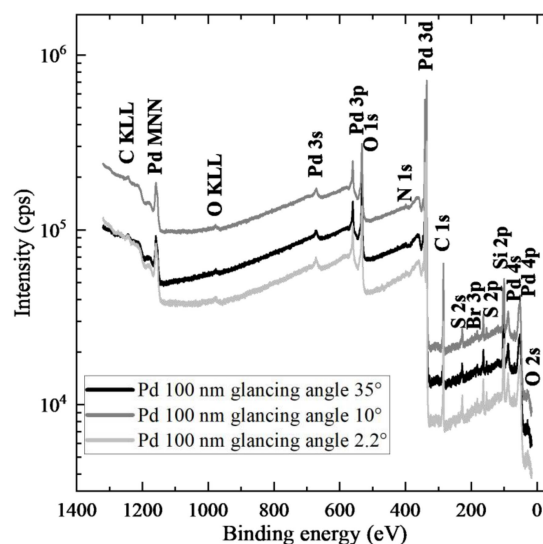


Fig. 4. XPS survey spectra of Pd 100 nm nanolayer for different glancing angles: 35°, 10°, and 2.2° (below the critical angle for Pd (2.37°)). The sample was irradiated by the monochromatized Al K_{α} photons. In the spectra, both photoelectron (Pd 3s, Pd 3p, O 1s, N 1s, Pd 3d, C 1s, S 2s, Br 3p, Si 2p, Pd 4s, Pd 4p, O 2s) and Auger peaks (C-KLL, Pd-MNN, O-KLL) were identified.

values, standard deviations, and the coefficients of variation. For the Pd nanolayer surface, the following mean element concentrations were achieved: palladium (37.7 at.%), silicon (22.6 at.%), carbon (26.4 at.%), oxygen (5.5 at.%), sulfur (4.1 at.%), nitrogen (3.5 at.%), and bromine (0.25 at.%). Standard deviations were in the range from 0.04 at.% (Br) to 2.3 at.% (Pd), resulting in a variation coefficient at

the level of 5–17%. The largest variation in concentration was observed for bromine (17%), probably due to low concentration, while the Pd concentration changed within about 6%.

For the Ti nanolayer surface, the following mean composition was obtained: oxygen (44.8 at.%), carbon (29.3 at.%), titanium (24.7 at.%), and nitrogen (1.2 at.%). Standard deviations were in the range

TABLE III

The detection limit for the XPS/TRXPS techniques obtained for photoelectron peaks identified at the surface of the Ti nanolayer (75 nm), based on the survey spectra registered for various glancing angles.

Photoelectron peak	Binding energy [eV]	FWHM [eV]	Limit of detection [at.%]		
			angle 35°	angle 10°	angle 1.5°
O 2s	21.5	2.79	1.229 ± 0.066	0.557 ± 0.020	0.298 ± 0.009
Ti 3p	36.7	2.67	0.452 ± 0.048	0.188 ± 0.020	0.084 ± 0.009
Ti 3s	61.6	4.44	1.396 ± 0.153	0.556 ± 0.060	0.276 ± 0.031
C 1s	284.8	1.53	0.275 ± 0.034	0.108 ± 0.012	0.048 ± 0.005
N 1s	399.3	1.25	0.120 ± 0.020	0.067 ± 0.010	0.036 ± 0.004
Ti 2p (Ti 2p _{3/2})	458.3	1.57	0.126 ± 0.012	0.047 ± 0.005	0.022 ± 0.002
O 1s	529.8	1.48	0.246 ± 0.006	0.103 ± 0.002	0.053 ± 0.001
Ti 2s	564.3	4.81	1.459 ± 0.145	0.611 ± 0.063	0.291 ± 0.032

from 0.15 at.% (N) to 3.0 at.% (C), which resulted in the variation coefficient at the level of 2–13%. The most significant variation in concentration was observed for nitrogen (13%), while the Ti concentration changed within about 9%.

3.3. XPS/TRXPS detection limit

The analysis of the XPS/TRXPS spectra, which focused on the photoelectron peaks intensity and the level of background, enabled estimating the detection limit (DL) of these techniques, which can be calculated using the following formula

$$DL = \frac{3C}{I_n} \sqrt{\frac{I_b}{t}}, \quad (2)$$

where C is the element concentration in the studied nanolayer probed by the XPS/TRXPS technique, I_n is the net intensity of the analyzed photoelectron peak, I_b is the background level under this peak, and t is the measurement dwell time.

Table III presents the detection limit achieved for element photoelectron peaks identified at the surface of the Ti nanolayer (75 nm) deposited on a silicon substrate, based on the survey spectra registered for 35°, 10°, and 1.5° (total reflection regime) angles. In the case of the Ti 2p photoelectron peak, the Ti 2p_{3/2} component was analyzed.

Table III also presents the binding energy and FWHM of the photoelectron peaks, calculated as the average of values from measurements performed for the discussed angles. The standard deviation for the mean value of the binding energy is at the level of 0.1 eV, while the standard deviation for the average value of the FWHM is about 0.4 eV. Element concentration needed for calculating DL was assumed as a mean value achieved from the survey spectra registered for angles 35°, 10°, and 1.5° (Table II).

In calculating the detection limits, the change in the surface area of the primary beam associated with the change in the glancing angle was taken into account. The ratio of the primary X-ray beam

area at 1.5° to the beam area at 35° reached approximately 22, while the ratio of the beam area at 2.2° to the beam area at 35° was approximately 15, and, finally, at 10° it was 3.3.

The obtained values of DL depend on the glancing angle and vary in range from 0.120 to 1.459 at.% for 35°, from 0.047 to 0.611 at.% for 10°, and, finally, from 0.022 to 0.298 at.% for 1.5°. It can be observed that the application of the primary X-ray beam total reflection reduces DL by a factor of about 3-6 compared to the classical XPS conditions.

Moreover, for the given element, e.g., Ti or O, the detection limit value depends on the type of the analyzed photoelectron peak and is the lowest for the strongest peak. In the case of titanium, it is the Ti 2p photoelectron peak, while for oxygen, it is O 1s.

The DL uncertainty was determined using the total differential method, taking as the uncertainty of the element concentration the standard deviation determined from the measurements of the survey spectra for different angles (Table II). The square root of the intensity was taken as the uncertainty of the intensity.

As can be seen in Table III, the relative uncertainty of the detection limit reaches 3–17%, with an average of 10%. Finally, the lowest value of detection limit, for the 75 nm Ti nanolayer, was achieved for the Ti 2p peak, for angle 1.5°, being equal to $0.022 \pm 0.002at.\%$.

Table IV presents the detection limits for element photoelectron peaks identified at the Pd nanolayer (100 nm) surface deposited on the silicon substrate, based on the survey spectra registered for 35°, 10°, and 2.2° (total reflection regime) angles. In the case of Pd 3p, the Pd 3p_{3/2} was analyzed. For Pd 3d, it was Pd 3p_{5/2}, and for Pd 4p, it was Pd 4p_{3/2}. Table IV also contains the values of the binding energy and the FWHM of photoelectron peaks, which were calculated as an average of values from the measurements performed for the discussed angles. The standard deviation for the mean value of the

TABLE IV

The detection limit for the XPS/TRXPS techniques obtained for photoelectron peaks identified at the surface of the 100 nm Pd nanolayer, based on the survey spectra registered for various glancing angles.

Photoelectron peak	Binding energy [eV]	FWHM [eV]	Limit of detection [at.%]		
			angle 35°	angle 10°	angle 2.2°
O 2s	23.0	0.40	1.354 ± 0.203	0.761 ± 0.115	0.340 ± 0.053
Pd 4p	51.5	8.16	0.847 ± 0.060	0.381 ± 0.026	0.228 ± 0.016
Br 3d	68.6	0.77	0.044 ± 0.007	0.021 ± 0.004	0.010 ± 0.002
Pd 4s	87.6	4.00	2.602 ± 0.193	1.188 ± 0.082	0.556 ± 0.039
Si 2p	99.8	0.99	0.526 ± 0.060	0.230 ± 0.022	0.153 ± 0.014
Br 3p	163.3	2.31	0.054 ± 0.009	0.022 ± 0.004	0.012 ± 0.002
S 2p	181.8	0.95	0.300 ± 0.020	0.118 ± 0.007	0.063 ± 0.004
S 2s	227.6	2.08	0.327 ± 0.022	0.176 ± 0.010	0.077 ± 0.004
C 1s	284.8	1.57	0.361 ± 0.020	0.143 ± 0.007	0.084 ± 0.004
Pd 3d	335.5	1.41	0.055 ± 0.003	0.022 ± 0.001	0.013 ± 0.001
N 1s	399.1	0.88	0.591 ± 0.043	0.282 ± 0.017	0.156 ± 0.010
Pd 3p	532.6	3.14	0.303 ± 0.019	0.123 ± 0.008	0.072 ± 0.005
Pd 3s	672.1	5.71	3.641 ± 0.251	1.297 ± 0.086	0.765 ± 0.052

binding energy was at the level of 0.3 eV, and the standard deviation for the mean value of the FWHM was also about 0.3 eV. Element concentration necessary for calculating DL was assumed as a mean value from the survey spectra registered for the following angles: 35°, 10°, and 2.2° (Table II).

As for the Ti nanolayer, the obtained values of DL depended on the glancing angle and varied from 0.044 to 3.641 at.% for angle 35°, from 0.021 to 1.297 at.% for 10°, and, finally, from 0.010 to 0.765 at.% for 2.2°. It can be observed that applying the primary X-ray beam total reflection reduced the DL by a factor of about 3–5 compared to the classical XPS conditions.

For Pd, the value of the detection limit depends on the type of analyzed photoelectron peak and is the lowest for the strongest peak Pd 3d (i.e., Pd 3p_{5/2}).

As can be seen in Table IV, the relative uncertainty of the detection limit was at 5–18%, with an average of about 10%. Finally, the lowest value of detection limit, for the 100 nm Pd nanolayer, was achieved for an angle of 1.5° (0.010 ± 0.002 at.%).

4. Conclusions

In the presented study, the X-ray photoelectron spectroscopy in the non-total and total reflection conditions was applied to analyze the Ti (75 nm) and Pd (100 nm) nanolayers deposited on Si substrate with magnetron sputtering. The survey spectra were registered for different glancing angles, i.e., 35°, 10°, and 2.2° for the Pd nanolayer and 1.5° for the Ti nanolayer. The analysis of the spectra concentrated on examining the binding energy, the FWHM, the intensity, and the background level for

the registered photoelectron peaks. The nanolayer surface homogeneity, defined by the variation coefficient of element concentration, was obtained as 2.3% for Ti and 14.7% for the Pd sample. The obtained detection limit for XPS/TRXPS was in the range from 0.010 to 3.6 at.%, depending on the glancing angle, nanolayer, and photoelectron peak of the detected element. In general, the application of total reflection X-ray photoelectron spectroscopy geometry improves the detection limit of the X-ray photoelectron spectroscopy technique by a factor of 3–6, depending on the analyzed nanolayer and the type of photoelectron peak.

Knowledge of the properties of the Ti and Pd nanolayer surfaces will be applied to interpret the results of the studies conducted at the Institute of Physics of Jan Kochanowski University, related to the formation of the nanostructures in the interaction of the highly charged xenon ions with nanolayers. The XPS/TRXPS analysis of other metallic nanolayers will serve as the continuation of the presented studies.

Acknowledgments

The equipment was purchased thanks to the financial support of the European Regional Development Fund in the framework of the Polish Innovative Economy Operational Program (contract No. WNPPPOIG.02.02.00-26-023/08) and the Development of Eastern Poland Program (contract No. POPW.01.01.00-26-013/09-04). The functioning of the facility is supported by the Polish Ministry of Education and Science (project 28/489259/SPUB/SP/2021).

This article is based upon work from COST Action CA18130 ENFORCE TXRF, supported by COST (European Cooperation in Science and Technology, www.cost.eu).

References

- [1] P. van der Heide, *X-ray Photoelectron Spectroscopy: An Introduction to Principles and Practices*, John Wiley & Sons, Hoboken (NJ) 2011.
- [2] D. Baer, M. Engelhard, *J. Electron. Spectrosc. Relat. Phenom.* **178–179**, 415 (2010).
- [3] R. Klockenkämper, A. Von Bohlen, *Anal. Bioanal. Chem.* **408**, 667 (2016).
- [4] J. Kawai, *J. Electron. Spectrosc. Relat. Phenom.* **178–179**, 268 (2010).
- [5] J. Kawai, M. Takami, M. Fujinami, Y. Hashiguchi, S. Hayakawa, Y. Gohshi, *Spectrochim. Acta B* **47**, 983 (1992).
- [6] J. Kawai, H. Amano, K. Hayashi, T. Horiuchi, K. Matsushige, Y. Kitajima, *Spectrochim. Acta B* **52**, 873 (1997).
- [7] A. Alshehabi, N. Sasaki, J. Kawai, *Spectrochim. Acta B* **114**, 34 (2015).
- [8] A. Kubala-Kukuś, D. Banaś, I. Stabrawa, K. Szary, D. Sobota, U. Majewska, J. Wudarczyk-Moćko, J. Braziewicz, M. Pajek, *Spectrochim. Acta B* **145**, 43 (2018).
- [9] H.P. Urbach, P.K. de Bokx, *Phys. Rev. B* **53**, 3752 (1996).
- [10] J. Baumann, Y. Kayser, B. Kanngießer, *Phys. Status Solidi B* **258**, 2000471 (2021).
- [11] P. Dutta, *Curr. Sci.* **78**, 478 (2000).
- [12] K. N. Stoev, K. Sakurai, *Spectrochim. Acta B* **54**, 41 (1999).
- [13] A. Kubala-Kukuś, D. Banaś, M. Pajek et al., *Acta Phys. Pol. A* **139**, 247 (2021).
- [14] I. Stabrawa, A. Kubala-Kukuś, D. Banaś, G. Pepponi, J. Braziewicz, M. Pajek, M. Teodorczyk, *Thin Solid Films* **671**, 103 (2019).
- [15] R. Stachura, D. Banaś, A. Kubala-Kukuś et al., *Nucl. Instrum. Method B* **536**, 126 (2023).
- [16] D. Banaś, Ł. Jabłoński, P. Jagodziński, A. Kubala-Kukuś, D. Sobota, M. Pajek, *Nucl. Instrum. Method B* **354**, 125 (2015).
- [17] I. Stabrawa, D. Banaś, A. Kubala-Kukuś et al., *Vacuum* **210**, 111860 (2023).
- [18] X. Liu, P. Chu, C. Ding, *Mater. Sci. Eng. R* **47**, 49 (2004).
- [19] S. Cao, D. Li, A.A. Uliana et al., Y. Jiang, J. Zhu, Y. Zhang, B. Van der Bruggen, *Appl. Catal. B* **323**, 22175 (2023).
- [20] M. Polívková, M. Valová, J. Siegel, S. Rimpelová, T. Hubáček, O. Lyutakova, V. Švorčíka, *RSC Adv.* **5**, 73767 (2015).
- [21] N. Kim, H.H. Cho, Y. Kim et al., *Int. J. Hydrog. Energy* **48**, 1234 (2023).
- [22] A. Naumkin, A. Kraut-Vass, S. Gaarenstroom, C. Powell, *NIST Standard Reference Database* **20**, Ve4. 4.1, 2012.
- [23] Center for X-Ray Optics, *X-Ray Properties of the Elements*.